

1-1-2007

Neutronics analysis of the high-power race target

Timothy E Beller

University of Nevada, Las Vegas

Follow this and additional works at: <https://digitalscholarship.unlv.edu/rtds>

Repository Citation

Beller, Timothy E, "Neutronics analysis of the high-power race target" (2007). *UNLV Retrospective Theses & Dissertations*. 2213.

<http://dx.doi.org/10.25669/u3cv-29yv>

This Thesis is protected by copyright and/or related rights. It has been brought to you by Digital Scholarship@UNLV with permission from the rights-holder(s). You are free to use this Thesis in any way that is permitted by the copyright and related rights legislation that applies to your use. For other uses you need to obtain permission from the rights-holder(s) directly, unless additional rights are indicated by a Creative Commons license in the record and/or on the work itself.

This Thesis has been accepted for inclusion in UNLV Retrospective Theses & Dissertations by an authorized administrator of Digital Scholarship@UNLV. For more information, please contact digitalscholarship@unlv.edu.

NEUTRONICS ANALYSIS OF THE
HIGH-POWER RACE TARGET

by

Timothy E. Beller

Bachelor of Science
University of Nevada, Las Vegas
2006

A thesis submitted in partial fulfillment
of the requirements for the

**Master of Science Degree in Materials and Nuclear Engineering
Department of Mechanical Engineering
Howard R. Hughes College of Engineering**

**Graduate College
University of Nevada, Las Vegas
December 2007**

UMI Number: 1452224

INFORMATION TO USERS

The quality of this reproduction is dependent upon the quality of the copy submitted. Broken or indistinct print, colored or poor quality illustrations and photographs, print bleed-through, substandard margins, and improper alignment can adversely affect reproduction.

In the unlikely event that the author did not send a complete manuscript and there are missing pages, these will be noted. Also, if unauthorized copyright material had to be removed, a note will indicate the deletion.

UMI[®]

UMI Microform 1452224

Copyright 2008 by ProQuest LLC.

All rights reserved. This microform edition is protected against unauthorized copying under Title 17, United States Code.

ProQuest LLC
789 E. Eisenhower Parkway
PO Box 1346
Ann Arbor, MI 48106-1346



Thesis Approval
The Graduate College
University of Nevada, Las Vegas

November 9, 2007

The Thesis prepared by

Timothy E. Beller

Entitled

Neutronics Analysis of the High-Power RACE Target

is approved in partial fulfillment of the requirements for the degree of

Master of Science in Materials and Nuclear Engineering

Examination Committee Chair

Dean of the Graduate College

Examination Committee Member

Examination Committee Member

Graduate College Faculty Representative

ABSTRACT

Neutronics Analysis of The High-Power Race Target

by

Timothy E. Beller

Dr. Daniel Cook, Examination Committee Chair
Professor of Mechanical Engineering
University of Nevada, Las Vegas

In this study, the neutron production of an electron accelerator target is analyzed. A large neutron flux is desired for transmutation research. Previously used targets were tested at 1 kW, but this particular target was designed to be used with powers up to 20 kW. In order to test the effectiveness of the design in creating neutrons, the target needed to be tested. The 20 kW beam was not available for testing so this target was tested at powers under 1 kW. The experiments were modeled using a particle transport code, MCNPX, and the target produced an average of 1×10^{12} neutrons/second in models. Almost all models produced ^{198}Au decay rates higher than the experimental results, which has also been seen in previous tests of the targets used on the Reactor Accelerator Coupling Experiments project.

TABLE OF CONTENTS

ABSTRACT.....	iii
LIST OF TABLES.....	vi
LIST OF FIGURES	vii
ACKNOWLEDGMENTS	viii
ACKNOWLEDGMENTS	viii
CHAPTER 1 INTRODUCTION	1
Problem.....	1
Scope.....	1
CHAPTER 2 REVIEW OF RELATED LITERATURE.....	3
Transmutation	3
Electron Accelerator Applications for Neutron Production.....	4
TRADE	4
Argonne National Lab Target	5
RACE Project.....	5
HP-RACE	6
CHAPTER 3 METHODOLOGY	8
Experiment.....	8
MCNPX Code.....	14
Geometry.....	14
Alternate Geometries	17
Materials	19
Tally Multiplier Card	20
Electron Energy Deposition.....	24
Neutron Energy Tally	25
Gold Foil Tallies	25
Weight Windows	26
Energy Cutoff Cards	28
CHAPTER 4 FINDINGS OF THE STUDY	30
Analysis of Data.....	30
Preliminary Modeling Results	34
Refined Model	40

CHAPTER 5 SUMMARY, CONCLUSIONS, AND RECOMMENDATIONS	43
Discussion of Results.....	43
Conclusions and Recommendations for Further Study	44
APPENDIX SAMPLE MCNPX INPUT AND OUTPUT FILES.....	46
VITA.....	55

LIST OF TABLES

Table 1	Gold foil positions as measured from the face of the target.	11
Table 2	Data collected from the electron beam characterization study.	12
Table 3	Material compositions used in MCNPX modeling of the HP-RACE.....	20
Table 4	Fraction of electron energy deposition per W-disk with a 23 MeV beam.....	31
Table 5	Results from the experimental gold activation measurements.	33

LIST OF FIGURES

Figure 1 Components of the HP-RACE target.....	7
Figure 2 HP-RACE staged in front of the beam window (left).....	8
Figure 3 Plot of the beam characterization test.	13
Figure 4 Cross-sectional view of MCNPX model.....	16
Figure 5 MCNPX model built with polyethylene bricks and the steel table.....	17
Figure 6 Neutron energy distribution in the HP-RACE target.	32
Figure 7 Decay rate comparisons between the experiment and the MCNPX model.	36
Figure 8 Decay rate comparison for Pb with different densities.	37
Figure 9 Decay rate comparisons for 20, 23.6 and 25 MeV models.	38
Figure 10 Decay rate comparisons for 23.6 MeV simple and complex models (low density Pb).	39
Figure 11 Decay rate comparisons for refined model.	42

ACKNOWLEDGMENTS

The author would like to thank Dr. Charlotta Sanders, Dr. Daniel Cook, Dr. Woosoon Yim, Dr. Julie Staggers, and the personnel of the Idaho State University Idaho Accelerator Center for their support and guidance. A great deal of appreciation is also due to my father, Dr. Denis E. Beller, for his expertise, support and a remarkable amount of patience throughout this learning experience.

CHAPTER 1

INTRODUCTION

Transmutation, or nuclear transformation, has gained interest as an effective way to deal with the problematic isotopes found in used nuclear fuel. This study evaluates the neutron production of a linear accelerator target that was designed for the specific application of accelerator-driven transmutation of used nuclear fuel [1].

Problem

This study investigates the neutron production of the High-Power Reactor Accelerator Coupling Experiments (HP-RACE) target [1]. By causing electrons to collide with a heavy metal target, it can produce photo-neutrons that can be used for transmutation of used nuclear fuel. Thus the main goal of any new accelerator target used to create neutrons in the same energy range as previous target designs should be increased neutron production.

Scope

The analysis of this target is limited to beam powers below 1 kW of ~23 MeV electrons, though the target was designed for up to 20 kW of beam power. The 20 kW

beam was not available at the time the experiments were performed. Theoretical models were built and analyzed using MCNPX 2.6D [2]. This target was designed and built prior to the beginning of this study; therefore no study was made of the use of different materials for the accelerator target.

CHAPTER 2

REVIEW OF RELATED LITERATURE

Transmutation

Transmutation is nuclear transformation which “converts volatile, radioactive isotopes into more stable isotopes by changing their nuclear structure” through radioactive decay, nuclear fission, fusion, or neutron capture [3]. One important parameter in transmutation technology is neutron production. In order for transmutation to occur via neutron capture or a fission reaction, a neutron must be provided to the nucleus so that it may become another isotope. For example, technecium-99, which is found in used fuel, is radioactive and has a half-life of ~211,000 years [4]. Bombarding technecium-99 with neutrons can induce neutron capture, which will create technecium-100, with a half-life of ~15.8s, which decays into stable ruthenium-100 very quickly [5]. Through this process, a long-lived radionuclide can be transformed into a non-radiotoxic, stable isotope.

Each radionuclide has several cross sections that describe the probability of different types of interaction. An absorption cross section, for example, can be broken down into a fission cross section and a radiative capture cross section. These cross sections describe the probability that an absorbed neutron will either be captured or will result in a

fission reaction and this leads to the reasoning behind seeking a high neutron production rate in transmutation technology. Given a probability of interaction, whether large or small, the overall probability of transmuting an atom increases as the number of neutrons passing the atom increases. This creates a need for a large number of neutrons/second passing through the isotope of interest.

Electron Accelerator Applications for Neutron Production

By coupling a heavy metal target with an electron linear accelerator, photo-neutrons can be produced through bremsstrahlung, or braking radiation. Through this reaction, electrons emit photons by depositing energy as they are slowed in a dense target. Provided these photons are of sufficient energy when they pass through another dense material, a neutron may be emitted. The energy required for this gamma-neutron reaction in specific materials used in this target will be discussed in the Methodology section. One of the benefits of using accelerators for transmutation is that they are portable and can be adapted to fit in many different existing facilities.

TRADE

The TRIGA Accelerator Driven Experiment (TRADE) was supposed to test the effectiveness of accelerator driven subcritical systems using a proton beam to generate neutrons for transmutation research [6]. The 2 mA proton cyclotron was designed to be coupled to a 1 megawatt TRIGA reactor and produce protons in the range of 110-140 MeV [6]. Studies were done to determine both the feasibility and efficiency of the

TRADE system for transmutation of minor actinides and fission fragments. This project ended prior to the finalization of experiments.

Argonne National Lab Target

A tungsten target was designed at Argonne National Lab to be used with electron energies between 100 and 200 MeV with a beam power of up to 100 kW [7]. The design is actually very similar to that of the HP-RACE target [1] with disks of tungsten that allow coolant to flow between them. This target produced around 2×10^{14} neutrons/second in the energy and power ranges for which it was designed. The peak energy of the neutrons was between 0.1 MeV and 1 MeV.

RACE Project

The RACE Project was started as a university transmutation research project under the Department of Energy's Advanced Fuel Cycle Initiative to study applications of accelerator driven subcritical systems [8]. The first tungsten target used on the RACE project was designed and successfully tested at Idaho State University's Idaho Accelerator Center (ISU-IAC) between 2003-2007. It was submerged in a tub of approximately 70 gallons of water, which provided all necessary cooling. This target, like all subsequent RACE targets, was 75% tungsten and 25% copper by weight. The neutron production from this target was $\sim 1 \times 10^{12}$ neutrons/second per kW of beam power [9].

A second target was designed to be coupled with the TRIGA reactor at the University of Texas at Austin [10]. This target had ½ inch diameter cooling lines that allowed cooling water to enter the target near its face. The water was pumped at ~ 2 gallons per

minute and a pressure of ~40 pounds per square inch. The neutron production was very similar to that of the original RACE target. It was successfully tested in August of 2005 at ~1.6 kW of beam power.

HP-RACE

The HP-RACE target shown in Figure 1 was engineered to withstand beam powers up to 20 kW in order to increase neutron production [11]. Due to the use of the increased power level over that used on previous RACE targets, a new target design was required with an innovative cooling system. Parametric studies of the copper-tungsten disk stack prior to the design of this target showed that the majority of electron deposition occurs within the first 0.5 cm of the target material. The copper-tungsten portion of the HP-RACE target consists of 7 disks of increasing thickness to allow for even electron energy deposition over all of the disks, which simplifies cooling. A cavity in the back of the target allows for the insertion of a uranium fuel rod for increased neutron production from fission induced by thermal neutrons. The target material is the same as that used in previous RACE targets so the expected neutron production per kW of beam power is expected to be very close to that of previous RACE targets, provided the fuel rod is not in place. The HP-RACE power level is ~20 times the power levels used in previous RACE tests, so the overall neutron production should increase by no less than an order of magnitude when the beam power is placed at 20 kW and the fuel rod is used.

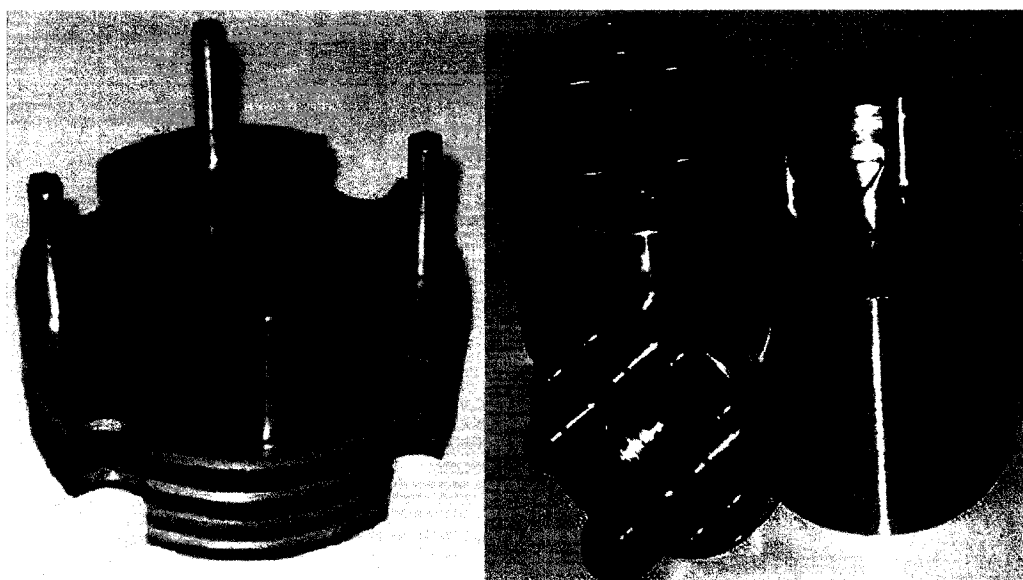


Figure 1 Components of the HP-RACE target; only part of the tungsten disk stack is shown to allow the alignment pins to be seen.

CHAPTER 3

METHODOLOGY

Experiment

The HP-RACE target was taken to the ISU-IAC for testing with an electron linear accelerator in August 2006. The beam was expected to produce from 20-25 MeV electrons, based on previous experiments [9]. The HP-RACE target was designed to be placed at the end of the accelerator's vacuum tube and did not attach to the tube. The electron beam passed through a 0.001 inch thick 304 Stainless Steel beam window before interacting with the target. An important issue faced during the setup of this experiment was making sure that the target was in-line with the vacuum tube and level with the beam window. As seen in Figure 2, a steel table, various sizes of polyethylene bricks and a small sheet of aluminum were used to level the target and align it with the beam tube.



Figure 2 HP-RACE staged in front of the beam window (left).

The target was originally designed to hold a small uranium fuel rod in the cavity at the rear of the target, but the rod was unavailable at the time of these experiments. The photons emitted by the interactions of the electrons in the tungsten target also need a dense material to produce photo-neutrons, so lead pellets were used to fill the cavity. Lead has a density of 11.34 g/cm^3 compared to 19.1 g/cm^3 for natural uranium [12]. The difference between the density of the uranium fuel rod and the lead is quite large, but the lead pellets were the only dense material available at the time of the experiments. Although there is very little uranium-235 found in natural uranium, any amount present is fissile. Lead is not a fissile material, so any neutron generation found in the experiment with the lead will be increased with the intended uranium fuel rod in place due to uranium-235's thermal neutron fission cross-section of 587 barns ($1 \text{ barn} = 10^{-24} \text{ cm}^2$) [12].

Gold foils were chosen as the material to be used to measure activation. When ^{197}Au absorbs a neutron it becomes ^{198}Au , which decays primarily by the emission of a 411 keV gamma ray (95.5%) [4]. These foils were readily available at the ISU-IAC, as was a gamma ray detector for counting the foils after the tests.

Plans had previously been made to test the target for 30 minutes for a separate thermal experiment with the following parameters:

- Frequency $90 \pm 1 \text{ Hz}$
- Pulse width $4 \pm 0.5 \mu\text{s}$
- Current $8 \pm 0.5 \text{ mA}$

At the time, the HP-RACE target had not yet been tested with parameters this high, so this was deemed a good time to activate the gold foils. The foils were placed at specific locations along the body of the target to provide a means for measuring neutron production through the activation of the foils. This also provided a means for comparing activation at very specific points, which allowed a more detailed comparison of results between models and experiments.

Assuming the top of the target is represented by 90° , foils were placed at 90° , 180° and 270° . The masses and positions of the foils as measured from the face of the target are given in Table 1. The foils placed at 180° and 270° provided information about the effects of the polyethylene blocks and the steel table on activation levels. The first foil at 90° , 180° and 270° were placed 0.25 cm from the face of the target. The 180° position had only one foil because it was assumed that there would only be a small difference between the sides and the top. The foils at the 270° position were placed every 7.62 cm (3 in) from the first foil (labeled L). The foils placed on the top of the target had a spacing of 2.54 cm (1 in) in order to provide more detailed information that could be compared to the modeling results.

Table 1 Gold foil positions as measured from the face of the target.

Top			Side			Bottom		
Foil Label	Position (cm)	Mass (g)	Foil Label	Position (cm)	Mass (g)	Foil Label	Position (cm)	Mass (g)
A	0.635	0.1278	K	0.635	0.1275	L	0.635	0.1267
B	2.858	0.1282				M	8.255	0.1273
C	5.398	0.1278				N	15.875	0.1274
D	7.938	0.1269				O	23.495	0.1272
E	10.478	0.1285						
F	13.018	0.1274						
G	15.558	0.127						
H	18.098	0.1275						
I	20.638	0.1274						
J	23.178	0.1274						

Once all foils were in place, the target was wrapped in bubble wrap for a separate thermal experiment and the beam was turned on for the scheduled 30 minute (1800 second) test. The run-time of the experiment was controlled manually by ISU-IAC personnel, so the beam time was actually 1827 seconds.

The gamma ray detector available at the ISU-IAC was a high-purity germanium (HPGe) detector. The germanium crystal was 7.9 cm in diameter and 9.75 cm long inside a lead pig to prevent interference from external radiation sources. The gold foils were placed into the HPGe detector one at a time, starting with the foils that were closest to the face of the target. The program used for counting the foils provided the counts per second as well as the relative error. All foils were counted until the percent standard deviation dropped below 2%.

While the gold foils were placed in the detector and counted, the electron beam was characterized. The amount of charge collected per energy bin was divided by the total amount of charge collected to determine the relative charge per energy bin (Table 2). The

sum of the product of each energy bin and its relative charge provided the average energy of the beam of 23.6 MeV. In Figure 3 the distribution of beam energy is shown.

Table 2 Data collected from the electron beam characterization study.

Energy (MeV)	Shot	Charge	Relative Charge	Energy (MeV)
17.0	1	0.853	0.00302	0.05
17.5	2	1.014	0.00359	0.06
18.0	3	1.114	0.00395	0.07
18.5	4	1.532	0.00543	0.10
19.0	5	1.612	0.00571	0.11
19.5	6	2.108	0.00747	0.15
20.0	7	2.482	0.00879	0.18
20.5	8	3.069	0.01087	0.22
21.0	9	3.928	0.01392	0.29
21.5	10	6.9	0.02445	0.53
22.0	11	16.74	0.05931	1.3
22.5	12	30.3	0.10735	2.4
23.0	13	40.3	0.14278	3.3
23.5	14	40.34	0.14292	3.4
24.0	15	35.78	0.12676	3.0
24.5	16	28.59	0.10129	2.5
25.0	17	20.96	0.07426	1.9
25.5	18	15.4	0.05456	1.4
26.0	19	10.95	0.03879	1.0
26.5	20	7.87	0.02788	0.74
27.0	21	5.57	0.01973	0.53
27.5	22	3.29	0.01166	0.32
28.0	23	1.36	0.00482	0.13
28.5	24	0.194	0.00069	0.02
Total		282.256	1.00000	23.646

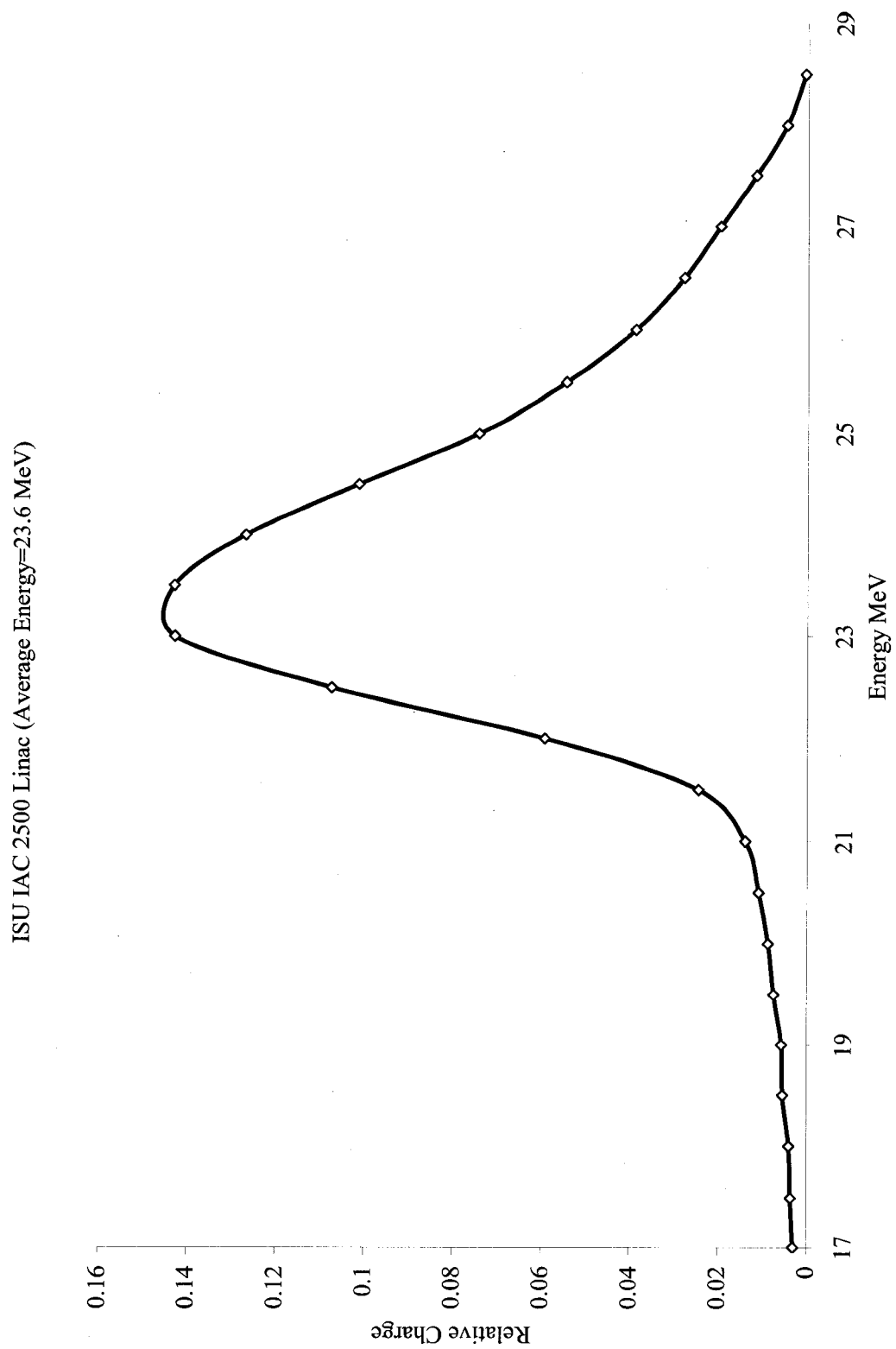


Figure 3 Plot of the beam characterization test.

Using the following equation and taking into consideration that the electron beam is pulsed, the power of the beam is found:

$$P = \text{Voltage} \times \text{Current}$$

$$P = 23.6 \text{ MeV} \times 0.08 \text{ A} \times 90 \text{ Hz} \times 4 \mu\text{s}$$

$$P = 680 \text{ W}$$

Though 680 W is much lower than the 20 kW of power that this target was designed for, the data collected during the experiment still provided a means for analyzing the neutronics of the target. The 680 W beam also provided sufficient gold foil activation to provide data for this study without excessive target activation.

MCNPX Code

The Monte Carlo particle transport code MCNPX, Version 2.6d, was used to model the HP-RACE experiment [2]. Version 2.5 of the MCNPX code has been benchmarked, validated, and verified in national and international studies for many years. The tests contained herein were modeled in Version 2.5 and compared to results from Version 2.6d to ensure that the results agreed prior to accepting Version 2.6d for further modeling.

Geometry

The HP-RACE geometry was modeled in two basic forms: with the polyethylene brick/steel table support shown previously in Figure 2 and also without any support. The purpose of the two different geometries was to determine the effect of the supporting materials on the model's performance.

The main body of the target was built using a 28.3 cm long right circular cylinder. The HP-RACE target was designed to divide the electron energy deposition evenly over the 7 tungsten disks by using disks of increasing thickness with the thinnest disk at the front of the target (1). The model was created using as-built disk thicknesses starting at the front of the target of 0.12, 0.13, 0.15, 0.18, 0.22, 0.29, and 0.41 cm for a total of 1.5 cm of tungsten in the portion of this target that was intended for photon production. The aluminum spacers that separate the disks and create water channels between them were modeled with as-built thicknesses of 0.25 cm.

The aluminum inlet and outlet water connections were modeled with an outer radius of 1.25 cm, an inner radius of 0.635 cm and they protrude from the face of the target by 2.55 cm. All water in the system was modeled as a union of individual water sections. Figure 4 provides a cross-sectional view of the front portion of the target where the water channels can be seen. The cavity in the rear of the target was 21.3 cm long with a diameter of 1.232 cm. Though the geometry reflects a cavity designed to hold a uranium fuel rod with a 0.036 cm aluminum sleeve, the calculations were not performed using the fuel rod.

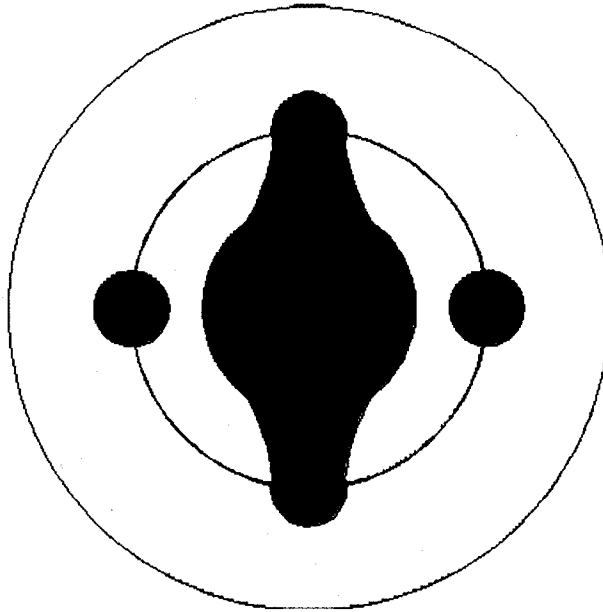


Figure 4 Cross-sectional view of MCNPX model; demonstrates the accurate representation of the coolant within the actual target.

In the experiments, the polyethylene bricks ranged in size from 15x10x5 cm to 15x10x10 cm. For models containing the support table and polyethylene bricks as shown in Figure 5, the bricks were modeled in MCNPX as one union of all of the polyethylene in the system. The aluminum sheet placed under the target for alignment with the beam tube was modeled at 0.32 cm thick. Only the top plate of the steel table was modeled, with a thickness of 0.507 cm. It was assumed that the legs would not have a significant contribution to the scattering of neutrons back into the target due to their size, location and orientation to the target. The entire geometry was surrounded with an air sphere of sufficient size to enclose all components.

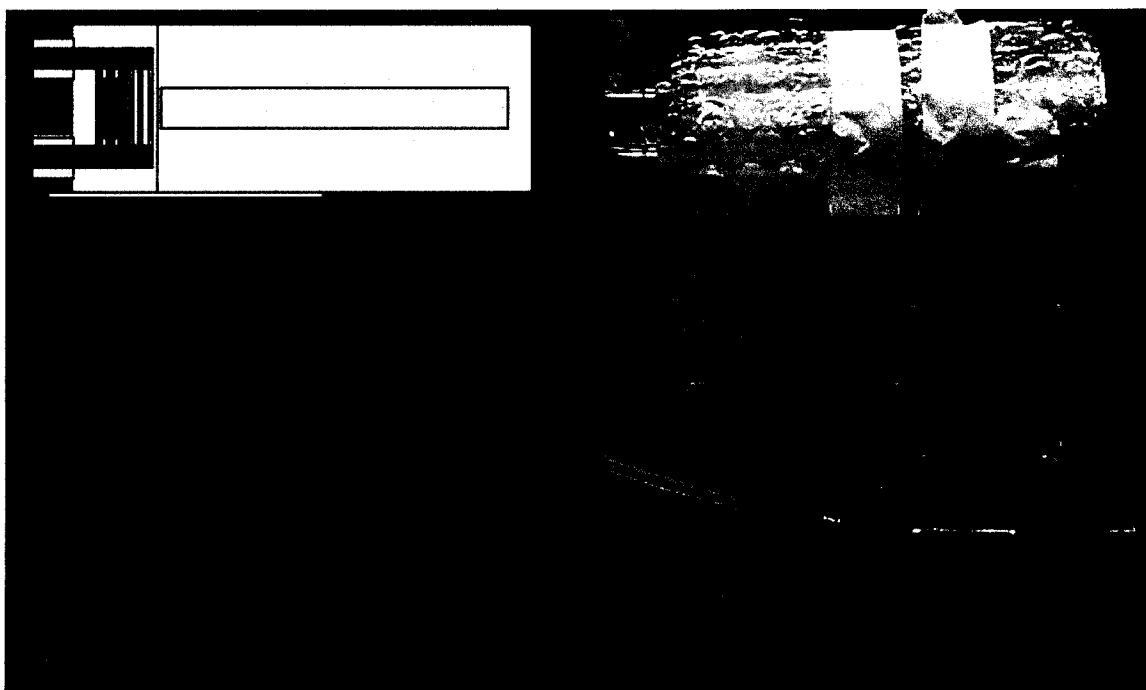


Figure 5 MCNPX model built with polyethylene bricks and the steel table.

Alternate Geometries

The main model used for all of the gold foil activation calculations was a 23.6 MeV electron beam with a fully specified geometry, including the steel table and the polyethylene bricks. The fully specified geometry contained borated polyethylene, which will be discussed in the Materials section. When modeled with the natural boron, this increases the neutron absorption in the polyethylene bricks and decreases neutron production. The bricks at ISU-IAC were specified as borated polyethylene, so the initial model was built to reflect this.

In order to test various combinations of materials and electron energies, a total of six models were created specifically for use with the gold foil activation runs. These were not used for the neutron energy or electron energy tests. The various models are as follows:

1. 20 MeV beam; steel table; borated polyethylene bricks; full density lead; aluminum sheet
2. 23.6 MeV beam; steel table; borated polyethylene bricks; full density lead; aluminum sheet
3. 25 MeV beam; steel table; borated polyethylene bricks; full density lead; aluminum sheet
4. 23.6 MeV beam; full density lead ; no steel, aluminum or polyethylene
5. 23.6 MeV beam; steel table; borated polyethylene bricks; aluminum sheet; low density lead
6. 23.6 MeV beam; steel table; aluminum sheet; full density lead; non-borated polyethylene

The low density lead models were created to account for the volume of air left in the rear cavity of the target by the spherical shape of the lead pellets. The mass of the lead pellets placed into the cavity was measured to be 0.70 ± 0.01 kg. The volume and density of the cavity were calculated as:

$$V = \pi r^2 h$$

$$V = \pi \times (1.232 \text{ cm})^2 \times 21.3 \text{ cm} = 101.6 \text{ cm}^3$$

$$\rho = \frac{\text{mass}}{\text{volume}}$$

$$\rho = \frac{0.70 \text{ kg}}{101.6 \text{ cm}^3} \times \frac{1000 \text{ g}}{1 \text{ kg}} = 6.9 \frac{\text{g}}{\text{cm}^3}$$

A density of 6.9 g/cm^3 for the lead in the cavity is significantly lower than the full density of lead at 11.34 g/cm^3 , so a model was built to test the effect this would have on photo-neutron creation. The non-borated polyethylene model was used to determine how the results would be altered if the bricks were, in fact, not borated. The model that was created without a steel table, polyethylene bricks or the aluminum sheet was used to determine the effect that these materials had on scattering around the target.

Materials

MCNPX results can be affected significantly by the use of improper materials, whether it is caused by incorrect isotopic compositions or from incorrect densities. For example, consider a system containing natural boron. The two naturally occurring isotopes of boron are boron-11 (80.1%) and boron-10 (19.9%), with thermal absorption cross-sections of 5.5 millibarns and 3840 barns, respectively (12). The very small absorption cross-section of boron-11 coupled with the fact that a large part of natural boron is boron-11 provides one example of how the expected dose to a person outside a given system could be significantly altered by not properly specifying the isotopes within the shielding material.

The materials used herein are replications of those used in the RACE project for the past several years. No attempt was made to alter these material compositions other than the addition or removal of the boron from the polyethylene. This was done because there was some confusion as to whether the polyethylene used in the experiment was truly borated. The only material that had its density altered was the lead in specific tests where it was required. The materials used in the models are shown in Table 3. Numbers shown

with a positive value are atomic fractions; those with a negative value are weight fractions. Of note, the boron percentage listed in Table 3 was an initial estimate as an actual value was never provided by the ISU-IAC personnel. A higher concentration was also tested and will be discussed.

Table 3 Material compositions used in MCNPX modeling of the HP-RACE

Material	Density (g/cm ³)	Isotope	Fraction	Isotope	Fraction
Water	1.00	O-16	1	H-1	2
Air	0.00129	N-14	79	O-16	21
Lead	11.35	Pb-208	1		
Copper- Tungsten	18.5	W-182	-0.198735	W-183	-0.1074
		Cu-63	-0.173	C-65	-0.07767
		W-184	-0.23	W-186	-0.2132
Aluminum	2.7	Al-27	98	Cr-52	0.04
		Cu-65	0.15	Fe-56	0.7
Gold	19.3	Au-197	1		
Steel	7.6	Fe	0.692	Mn-55	0.0107
		Ni	0.107	Cr	0.19
Polyethylene	0.96	H-1	0.66625	C	0.33325
		Natural B	0.00007		

Tally Multiplier Card

MCNPX results are provided per source particle, so the program provides a means for multiplying an answer by many different values. For example, a flux tally across a cell that is given in neutrons/cm² per source particle can be multiplied the number of source particles to put the results in terms of only the number of neutrons/cm². The tally multiplier card can also be used to produce results that have already been modified by

interaction probabilities, or cross-sections. For the model of the HP-RACE target, one of the goals is to compare the activation of the gold foils from the experiment with those from the model. As discussed previously, the gamma ray that was counted in the HPGe detector is emitted during the decay of ^{198}Au . The material used in the model for the gold foil is ^{197}Au , so the results need to be modified to include the likelihood that the ^{197}Au will, in fact, absorb a neutron. The multiplier card used in this study looks like this:

Fm5 3.64E+08 3 102

This card tells the code to apply these settings to the f5 point detector tally (discussed later) through the specification of the “5”. The “102” in the multiplier card causes the code to multiply the result by the cross-section of ^{197}Au (material “3” in this case) that deals with the probability of a neutron-gamma (n, γ) reaction. By multiplying by the fraction of the reactions that are caused by absorption of a neutron and the subsequent emission of a gamma, the result is changed from the number of neutrons crossing the ^{197}Au cell into the number of atoms of ^{198}Au created. The tally at this point is in units of barns/cm² per source particle. The experimental results were all taken in ^{198}Au decays/second, so MCNPX results need to be the same to allow comparison. To look at the results in units of ^{198}Au decays/second, the multiplier needs to be in terms of:

$$\frac{\text{atoms of gold} - 198 \times \text{cm}^2 \times \text{electrons}}{\text{barns} \times s}$$

The “3.64E+08” portion of the multiplier card is the multiplicative constant used to get the final answer into the units of atoms of ^{198}Au decays/second. It was calculated in the following manner, by first finding the current:

$$\text{Current} = \frac{0.8 \text{ amps} \times 90 \text{ Hz} \times 4\mu\text{s}}{1 \times 10^6 \frac{\mu\text{s}}{\text{s}}} = 2.88 \times 10^{-5} \frac{\text{Coulombs}}{\text{s}}$$

$$\text{Current} = 2.88 \times 10^{-5} \frac{\text{Coulombs}}{\text{s}} \times \frac{1 \text{ electron}}{1.602192 \times 10^{-19} \text{ Coulombs}} = 1.80 \times 10^{14} \frac{\text{electron}}{\text{s}}$$

This provides the necessary electron current crossing the target face that is needed to deal with the code-provided units of per source particle. The next step was to find the atom density of the ^{198}Au . Given the atomic weight of ^{198}Au as 197.9682252 grams/mole [4], the atom density was calculated as:

$$N = 6.02 \times 10^{23} \frac{\text{atoms}}{\text{mole}} \times \frac{\text{mole}}{197.9682252 \text{ grams}} \times 19.3 \frac{\text{grams}}{\text{cm}^3} = 5.87 \times 10^{22} \frac{\text{atoms}}{\text{cm}^3}$$

Converted into the necessary units of atoms per barn-cm gives:

$$N = 5.87 \times 10^{22} \frac{\text{atoms}}{\text{cm}^3} \times 1 \times 10^{-24} \frac{\text{cm}^2}{\text{barns}} = 5.87 \times 10^{-2} \frac{\text{atoms}}{\text{barn cm}}$$

The volume of the gold foils is:

$$V = \pi r^2 h$$

$$V = \pi \times (0.635 \text{ cm})^2 \times 0.005 \text{ cm} = 0.00633 \text{ cm}^3$$

Multiplying the atom density, the volume and the current in the correct units gives:

$$\begin{aligned} \text{Tally Multiplier} &= 5.87 \times 10^{-2} \frac{\text{atoms}}{\text{barn cm}} \times 1.80 \times 10^{14} \frac{\text{electron}}{\text{s}} \times 0.00633 \text{ cm}^3 \\ &= 6.68 \times 10^{10} \frac{\text{atoms cm}^3 \text{ electron}}{\text{barn cm s}} \end{aligned}$$

This constant does not yet take into account the amount of time the beam was turned on and has not accounted for the decay of the ^{198}Au . The half-life of ^{198}Au is 2.69 days [5] and the decay constant was calculated as:

$$\begin{aligned} T_{1/2} &= \frac{\ln(2)}{\lambda} \text{ (Lamarsh, 23)} \\ \lambda &= \frac{\ln(2)}{T_{1/2}} = \frac{\ln(2)}{2.69 \text{ days}} \times \frac{1 \text{ day}}{24 \text{vh}} \times \frac{1 \text{ h}}{3600 \text{ s}} = 2.98 \times 10^{-6} \text{ s}^{-1} \end{aligned}$$

With an experimental run time of 1827 seconds, the final constant for use on the tally multiplier card becomes:

$$\begin{aligned}\text{Tally Multiplier} &= 6.68 \times 10^{10} \frac{\text{atoms cm}^3 \text{ electron}}{\text{barn cm s}} \times 2.98 \times 10^{-6} \frac{1}{\text{s}} \times 1827 \text{ s} \\ &= 3.64 \times 10^8 \frac{\text{atoms cm}^3 \text{ electron}}{\text{barn cm s}}\end{aligned}$$

With this tally multiplier constant, the MCNPX cell tally flux results for the gold foils are output in the units of ^{198}Au decays per second, which allows the direct comparison of experimental and modeled results.

Electron Energy Deposition

The intent of the designers of the HP-RACE target was to spread out the electron energy deposition across all seven disks to allow for a simpler cooling system design. By decreasing the amount of energy deposited in the disks closer to the front, the amount of heating is also decreased. The disks further back then need to have their thickness increased in order to absorb the electrons and produce the photons that are needed for neutron production. If this is done correctly, the electron energy deposition in all 7 disks will be equal.

An energy deposition tally (f6 tally) was set up to test the design of the tungsten disk stack. A 23.6 MeV electron beam in the form of a point source was modeled on the face of the target. Each disk was tallied for electron energy deposition and the results were compared. The results of these tallies are in units of MeV per gram per source particle by default. The previously mentioned tally multiplier card was not used for these tallies, as the actual values are not of importance. The goal was to find out the *ratio* of the energy deposited in each disk and units do not affect that, provided all the units are the same.

Neutron Energy Tally

The use of any system designed to produce a given type of particle will most likely rely on a specific energy range of those particles. The purpose of the HP-RACE target is to produce neutrons, but there is also a desire to know at what energy those neutrons are leaving the target. The activation of anything outside the target, gold foils in our case, also relies on the neutron energies. The cross-sections of a material change as the energy of particles interacting with it change.

One model of the HP-RACE target was specifically set up to determine the energy spectrum of the neutrons within the system. A surface flux tally (f2 tally) was used with energy bins to determine the relative number of particles per energy bin crossing the outer radius of the aluminum body. Any flux tally could have been used because, like the electron energy deposition tally, the actual flux values are not of great concern here. The goal in this model was to determine the amount of particles in each energy bin relative to the total number of particles in all bins. Again, the tally multiplier was not used for this tally. Several initial models were created to determine the range of energy bins that should be used and each successive model was more detailed than the previous one. The final run was done with energy bins between 1×10^{-8} and 1 MeV.

Gold Foil Tallies

The gold foils were modeled as right circular cylinders with a thickness of 0.005 cm and a radius of 0.635 cm, which are the specifications provided by the ISU-IAC. They were placed at the same locations as the ones in the actual experiments. In order to find gold foil activation, the neutron flux across the foils needed to be determined. The initial

MCNPX calculations contained cell flux (f4) tallies over the gold foils. In order for MCNPX to produce acceptable statistics in the results, a large number of particles needed to cross the gold foils. The small volume used for this tally produced poor statistics, which then required long computer execution times. Additionally, the very small neutron-gamma cross section of ^{197}Au in the thermal energy range made the results unreliable. The neutrons that were reaching the gold foils were being multiplied by a very small probability of interaction, which was catastrophic for the statistics.

The final calculations were performed using point detector flux tallies (f5) at the center of the foils. This type of tally uses an exclusion radius that prevents particles that are created very close to the point detector from causing deviations in statistics [2]. The exclusion radius cannot cross over two different materials within the geometry without causing errors in the results. The small thickness of the gold foils and their close proximity to the aluminum body of the target made it very difficult to use this tally in conjunction with the foils; therefore, the foils were removed. The tally multiplier card was multiplying the flux at a point by the neutron-gamma cross section of ^{197}Au , so the gold material was not necessary. The only value needed to determine the amount of gold activation was the flux at that point. This provided far better statistics than the f4 tally with the multiplier card.

Weight Windows

A significant issue in these simulations was getting acceptable statistics in the foils throughout the length of the target. There were simply not enough particles getting to the rear of the target to create interactions that would place significant amounts of neutrons

into the gold foil cells. Initial tests had the flux in the last foil with ~95% relative error with a source of 100 million particles. MCNPX has a default maximum number of source particles of 1 billion, so increasing the source to its maximum still would not have been acceptable. In addition to the limit on the number of source particles, the computation time required to increase the source by a factor of 10 would have been exorbitant. There simply was not enough time or allowed particles to provide relative errors below 10%, which is the value that the MCNPX developers have set as a minimum relative error for certainty in results [2].

The solution used to obtain the desired statistics was the weight window generator provided in MCNPX. It essentially “pulls” particles toward a specified point by reducing their relative “weight” and increasing their number. The result is far better statistics. For the weight window generation file, the geometry was run with no steel table and no polyethylene bricks. The 23.6 MeV electron source was started on the face of the target and a point detector was placed behind the aluminum section that divides the rear of the target from the water channels. The weight window generator optimized the weight of all particles to produce the best statistics at this point detector. For the next run, the detector was moved 2 cm closer to the back of the target and, again, the particles were pulled toward the detector. Each successive run used the weight windows created in the previous run as a starting point. This was repeated until the detector was within 4 cm of the last foil. In order to pull the particles to the last foil, the vertical position was changed in the last two runs. This was done to increase the likelihood of getting neutrons to the foils at the back of the target to provide better statistics.

Energy Cutoff Cards

The MCNPX code allows the user to specify energy cutoff cards, which prevents the code from monitoring the particles below the energy cutoffs. Depending on the geometry, source and materials, this can save significant computational time. Using cutoff cards should not affect the accuracy of the results, provided the user is sure that the system will not be significantly impacted by ignoring particles below the energy specified.

In order for a photo-neutron to be emitted in the tungsten or lead, the photon must be of greater energy than the binding energy of the nucleus. As shown in Krane [13], the binding energy for elemental tungsten with a $Z=74$, $N=110$, and 184 nucleons per nucleus is:

$$\begin{aligned}\text{Binding Energy} &= [Z \times m(^1\text{H}) + N \times m_n - m(^A\text{X})] \times 931.5 \frac{\text{MeV}}{\text{u}} \\ \text{Binding Energy} &= \frac{[(74 \times 1.00794 \text{ u}) + (110 \times 1.00866501 \text{ u}) - 183.84] \times 931.5 \frac{\text{MeV}}{\text{u}}}{184 \frac{\text{nucleons}}{\text{nucleus}}} \\ \text{Binding Energy} &= 8.610 \frac{\text{MeV}}{\text{nucleon}}\end{aligned}$$

For elemental lead with a $Z=82$, $N=125$, and 207 nucleons per nucleus, the binding energy is calculated as:

$$\begin{aligned}\text{Binding Energy} &= \frac{[(82 \times 1.00794 \text{ u}) + (125 \times 1.00866501 \text{ u}) - 207.2] \times 931.5 \frac{\text{MeV}}{\text{u}}}{207 \frac{\text{nucleons}}{\text{nucleus}}} \\ \text{Binding Energy} &= 6.904 \frac{\text{MeV}}{\text{nucleon}}\end{aligned}$$

As shown in the calculations, photons below ~ 7 MeV should not have a significant effect on the production of photo-neutrons in either of these dense materials, so they were eliminated from the calculations.

CHAPTER 4

FINDINGS OF THE STUDY

Analysis of Data

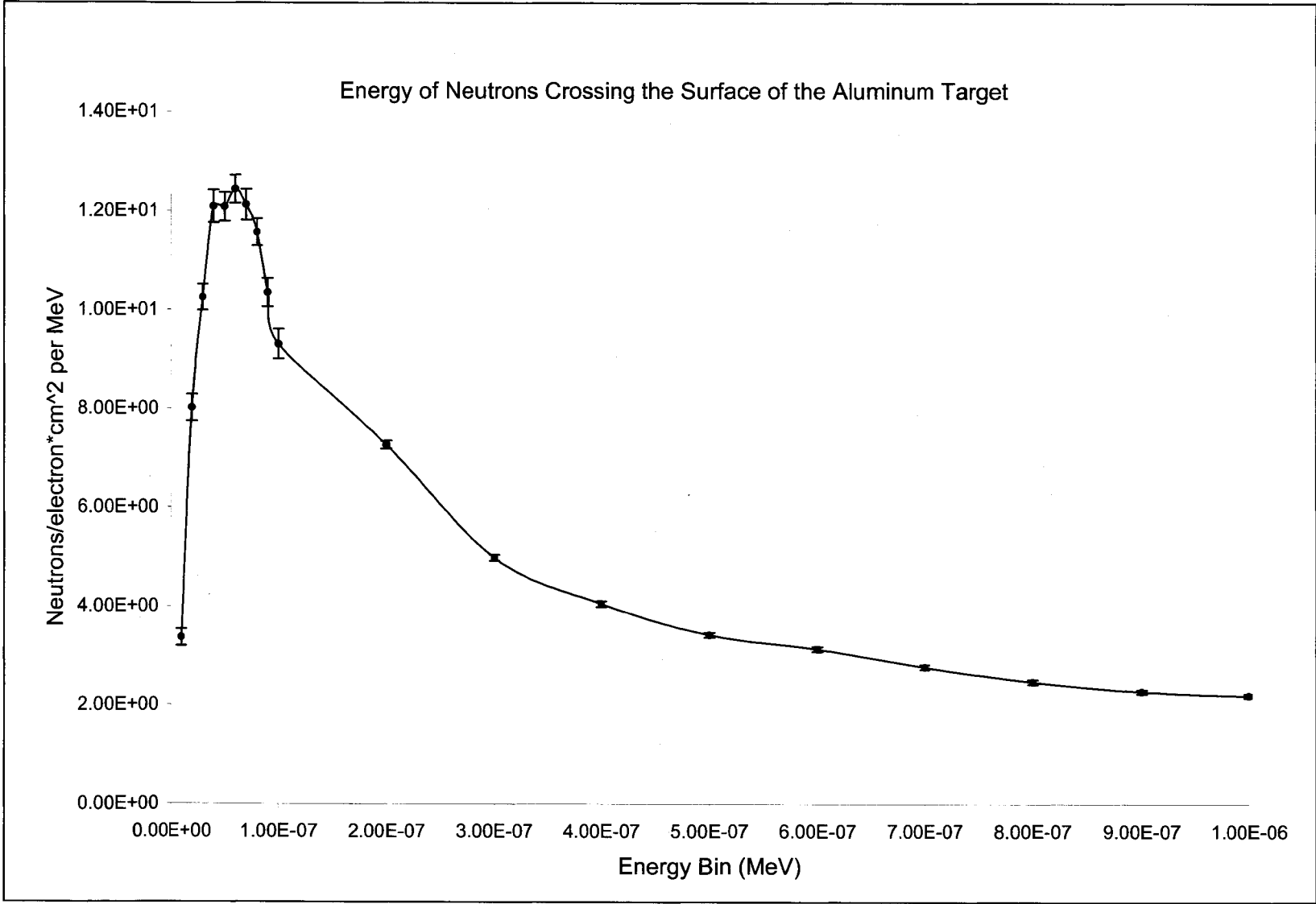
The results of the electron energy deposition study shown in Table 4 demonstrate that the designers of the target did not achieve their goal of even energy deposition. The values produced by the f6 tally in MCNPX for each disk were divided by the sum of the values for all disks to determine their relative energy deposition. All values had relative errors below 2% except the last two disks. MCNPX developers specify a relative error of 10% or lower as one of the requirements for passing statistical checks required to provide certainty of results [2]. The relative amount of electrons interacting in the last two disks was so low that good statistics were simply not possible. The first disk that the electrons cross absorbed 44% of the energy, with another 39% absorbed in the second disk. With five disks remaining, it is not difficult to see that the design was not effective in spreading out energy evenly. The first three disks absorbed 99% of the total electron energy absorbed by all of the disks.

Table 4 Fraction of electron energy deposition per W-disk with a 23 MeV beam.

Disk Position	Thickness (cm)	F6 Tally (MeV/g-source particle)	Relative Error	Relative Energy Deposited
1	0.12	8.34E+00	0.0001	0.44
2	0.13	7.34E+00	0.0001	0.39
3	0.15	2.93E+00	0.0001	0.16
4	0.18	2.65E-01	0.0005	0.01
5	0.22	3.58E-04	0.0120	0.00
6	0.29	8.08E-09	1.0000	0.00
7	0.41	0.00E+00	0.0000	0.00

The results of the neutron energy tally shown in Figure 6 demonstrate that the majority of the neutrons leaving the aluminum target are low energy. Though there are certainly higher energy neutrons, the amount of those is relatively low in comparison to the lower energy neutrons. This is good from the perspective of activation of the gold foils in the system due to its thermal absorption cross-section. If fast neutrons were desired by the designers, the HP-RACE target might not be the best solution, at least not in the configuration that was tested herein. With the addition of the uranium in place of the lead pellets, the energy of the neutrons escaping the aluminum body of the target will be significantly increased, though, due to the energy of the neutrons emitted from the fuel rod. The average number of neutrons released per fission event in uranium-235 is 2.418 with an average energy of 5 MeV for those neutrons [12]. This means that each neutron created per fission has ~2 MeV of energy, which is much higher than the neutrons produced in this experiment.

Figure 6 Neutron energy distribution in the HP-RACE target.



When the gold foils were measured using the HPGe detector, the values produced by the program were not automatically corrected for the detector efficiency and the probability that a 411 keV gamma ray would be produced. The ISU-IAC personnel provided a calibrated detector efficiency of 2.38%. The following equation converts the measured quantities into the actual decay of ^{198}Au :

$$\text{Actual Decay} = \frac{\text{gammas counted}}{s} \times \frac{\text{gamma produced}}{0.0238 \text{ gammas counted}} \times \frac{\text{decay}}{0.955 \text{ gammas produced}}$$

$$\text{Actual Decay} = 52.69 \frac{\text{Counts}}{s} \times \frac{1}{0.0238} \times \frac{1}{0.955}$$

$$\text{Actual Decay} = 2320 \frac{\text{Au} - 198 \text{ decays}}{s}$$

The results of the gold foil measurements shown in Table 5 clearly demonstrate that the foils positioned at the front of the target had a higher neutron flux than those at the back of the target. This was expected due to absorption of the photons as they proceed through the tungsten and the lead pellets.

Table 5 Results from the experimental gold activation measurements.

Foil Label	Position from target face (cm)	Counts/s	Detector Efficiency	Probability	Actual Au-198 decays/s
A	0.635	52.69	0.0238	0.955	2318.32
B	2.858	64.87			2853.98
C	5.398	48.31			2125.61
D	7.938	34.01			1496.38
E	10.478	23.37			1028.35
F	13.018	15.97			702.70
G	15.558	11.81			519.73
H	18.098	8.33			366.31
I	20.638	5.86			257.80

Preliminary Modeling Results

All of the previously mentioned models were used in MCNPX calculations to create trends that could be used to further refine the models. In Figure 7 the results from the experiment are compared to the 23.6 MeV MCNPX that contains the borated polyethylene bricks, the steel table and the low density lead. Error bars are presented on each plot. The decay rates found in the models are much higher than those in the experiment, which agrees with results from past experiments [14].

The model that used low density lead is compared to the full-density lead to determine the effect the lead density had on the neutron production (Figure 8). The model with the higher density lead produced results that are closer to the experimental results than the low density lead model.

The MCNPX calculations that were performed at 20, 23.6 and 25 MeV with full geometries containing borated polyethylene, the steel table and full-density lead are shown in Figure 9. The 20 MeV beam model produced results that were closer to experimental values than those produced by the higher energy models. The difference between the 20 and 23.6 MeV cases is nearly double the energy difference between the 23.6 and 25 MeV cases and the results reflect this. Error bars are not shown on the 25 MeV case due to the fact that they overlap the 23.6 MeV values.

The complex model containing the steel table and polyethylene blocks was compared to the model that only contained the target. Both models contained low density lead, but this does not change the difference seen in the decay rates in Figure 10. Up to this point in the study, of all the models created, the model that did not contain the table and plastic

bricks most closely matched the shape of the experimental plot, although the values are much higher than the experimental measurements.

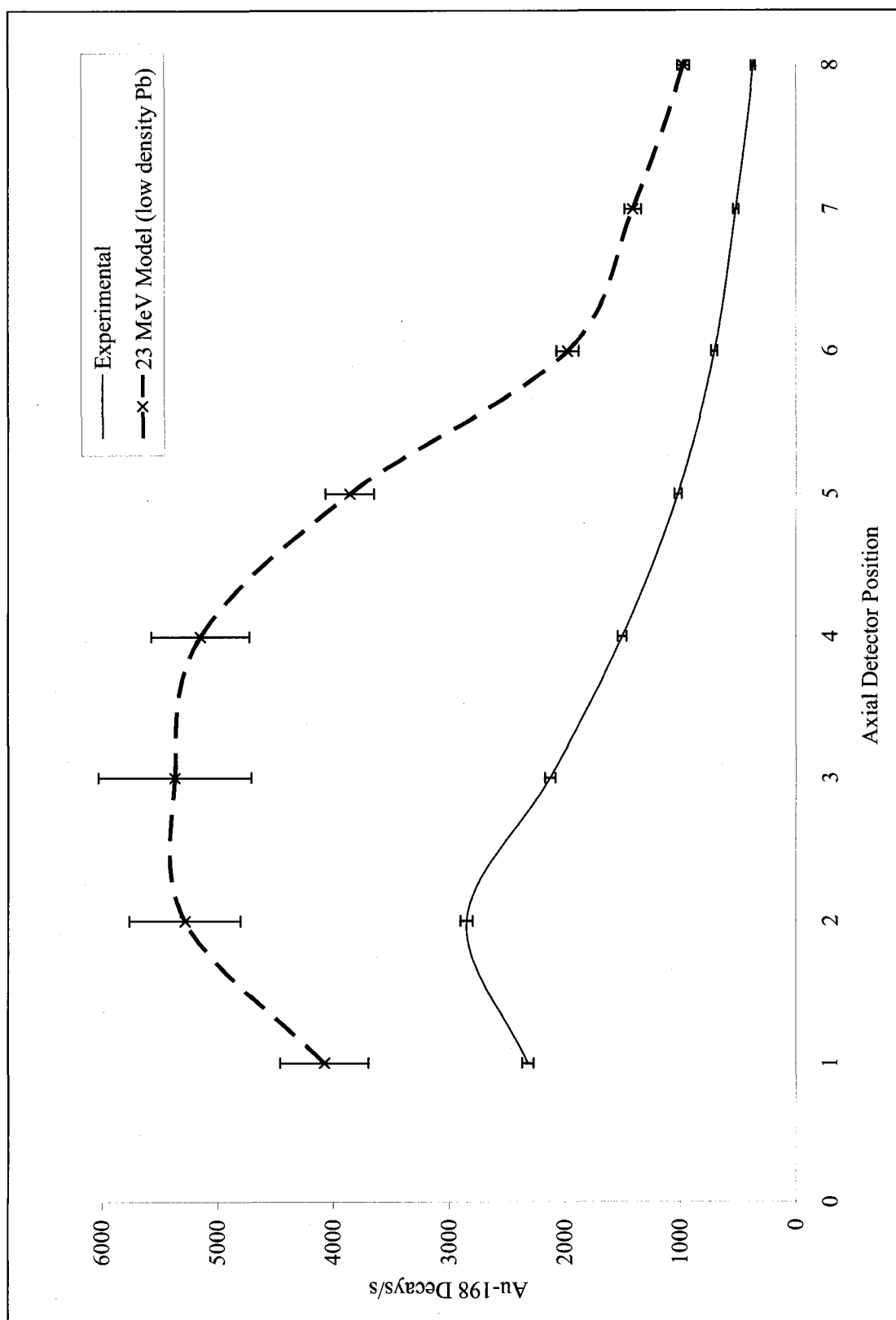


Figure 7 Decay rate comparisons between the experiment and the MCNPX model.

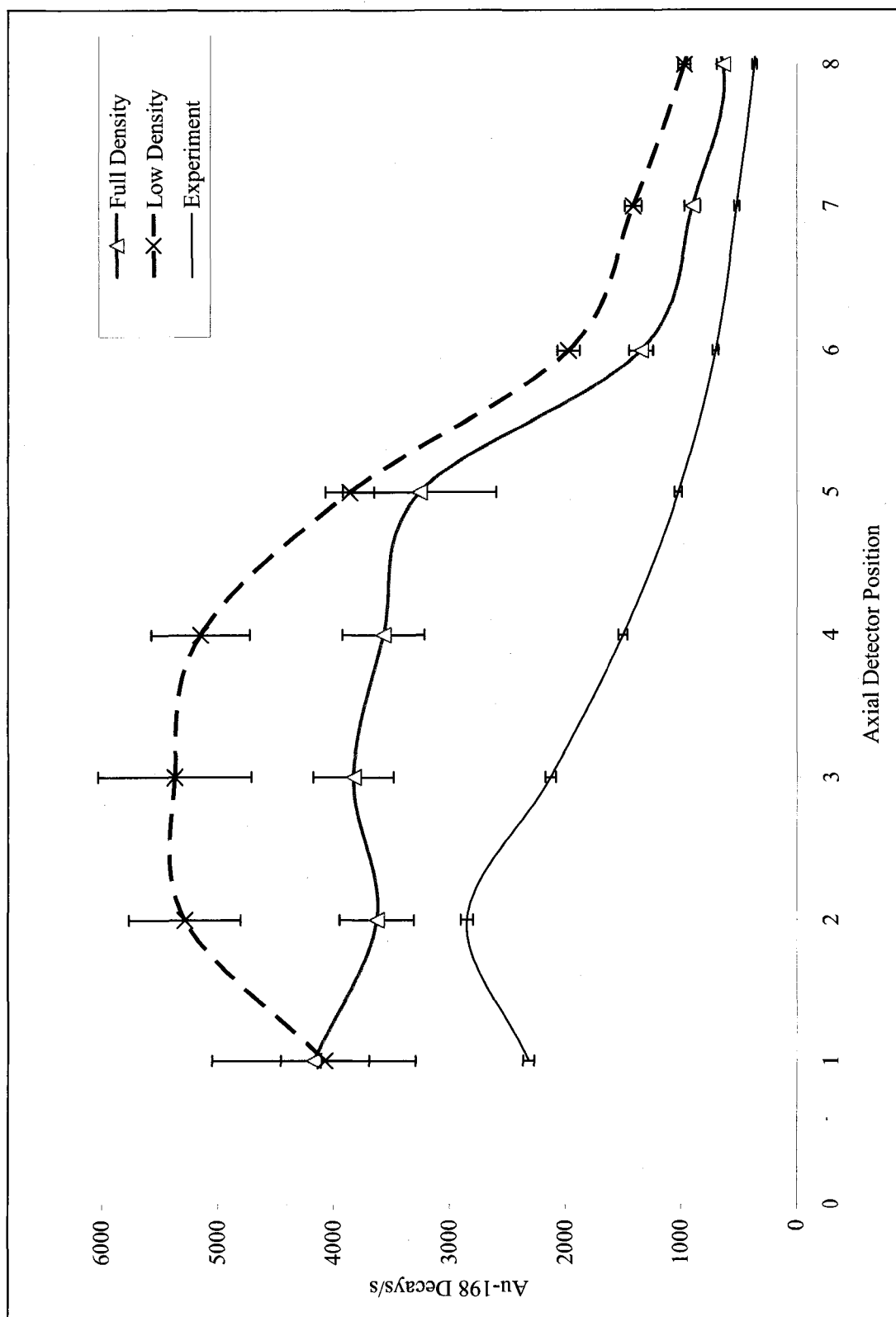


Figure 8 Decay rate comparison for Pb with different densities.

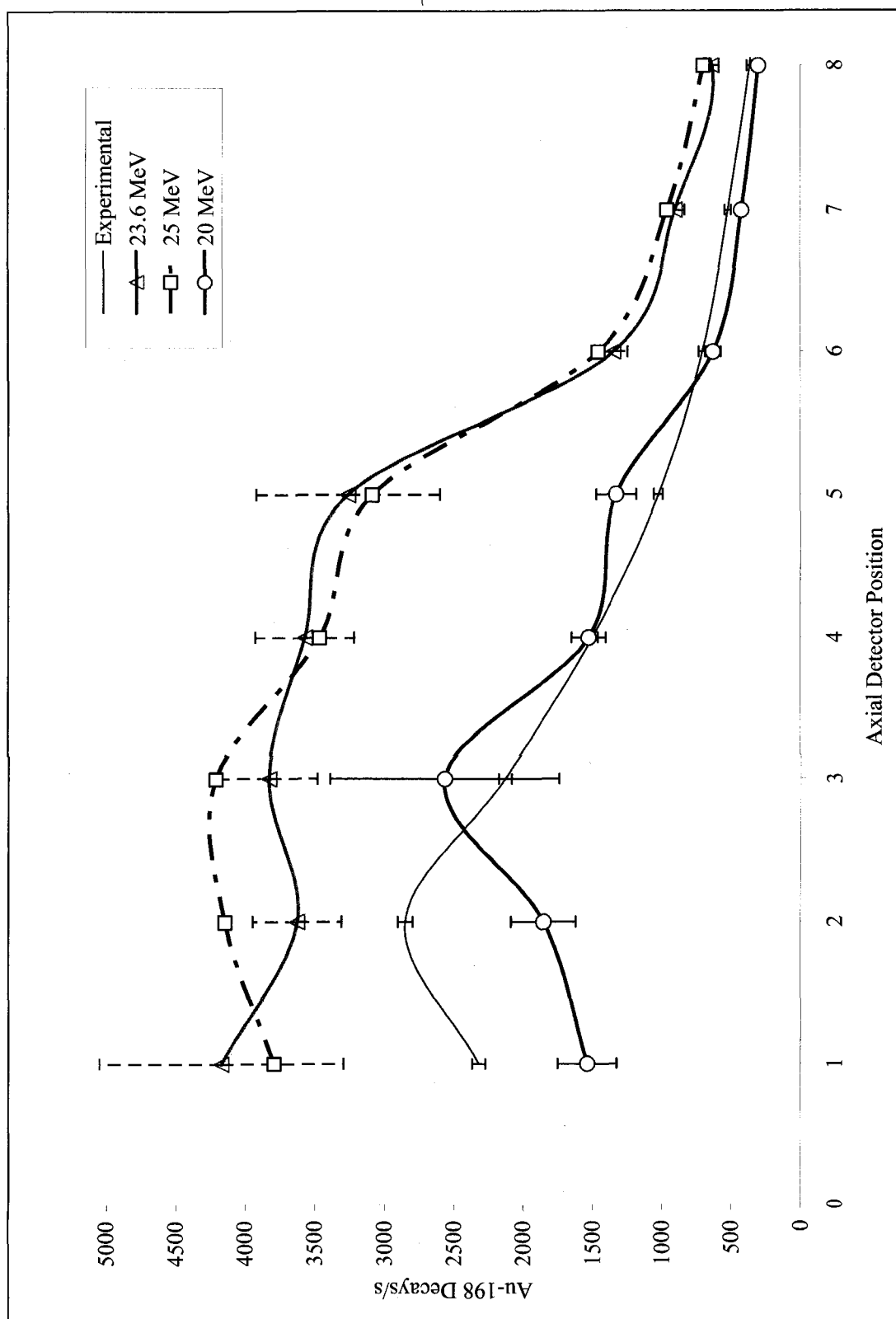


Figure 9 Decay rate comparisons for 20, 23.6 and 25 MeV models.

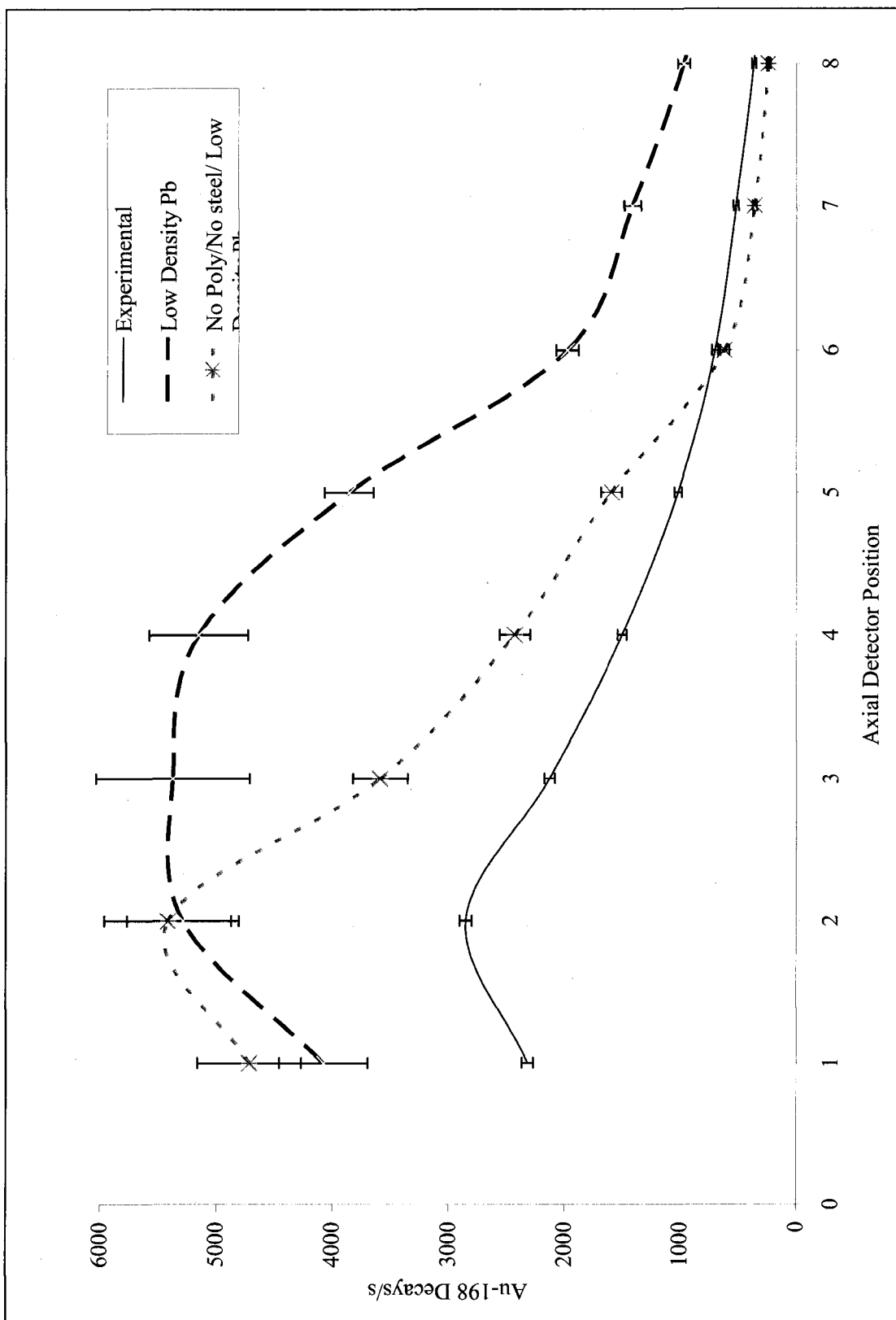


Figure 10 Decay rate comparisons for 23.6 MeV simple and complex models (low density Pb).

Refined Model

Though all of the results thus far have high relative errors and can not be used in an ideal comparison between experiments and models, they provide a great deal of information for the creation of a more refined model. The lack of information about the percentage of boron in the polyethylene used at the ISU-IAC was a serious hindrance in the accurate modeling of this experiment. This was an important variable in this study because of the neutron absorbing properties of boron.

Research was done on radiation shielding polyethylene to determine boron concentrations that are actually used in the nuclear field. One company provides borated polyethylene shielding material to the nuclear industry in boron weight percentages from 5% to 30% [15]. The 5% by weight borated polyethylene (10% atom fraction) was chosen for further study because it has a far higher concentration of boron than that previously used in this study ($7 \times 10^{-6}\%$ atom fraction). The atom fractions in this material are 56.3% hydrogen, 10% boron, 28.1% carbon and 5.6% oxygen with a density of 0.96 g/cm^3 .

The results shown in Figure 9 suggest that, although the relative errors are high, the most accurate model will have a beam energy of somewhere between 20 and 23.6 MeV. At this point in the study, the energy distribution provided by the beam study was revisited. It was determined that it would be beneficial to model the full distribution of the electron beam energy rather than to use the average. The final calculations for this study were performed in a very short period of time, so only the first few gold foils were modeled to cut down on calculation time. The results of foils 1, 2 and 3 are shown in Figure 11 with error bars. This model appears to have finally achieved good agreement

between MCNPX and experiments. The relative errors on foil 1, 2, and 3 for Figure 11 are 14%, 6% and 10%. Though the first foil cannot be seen as an accurate value without a slightly lower error, it is included in the plot to provide an idea of how well this model agrees with the experiment.

This refined model was also tested with a natural uranium fuel rod in place of the lead pellets. In this model, the neutron production of the HP-RACE target increased by a factor of 2.

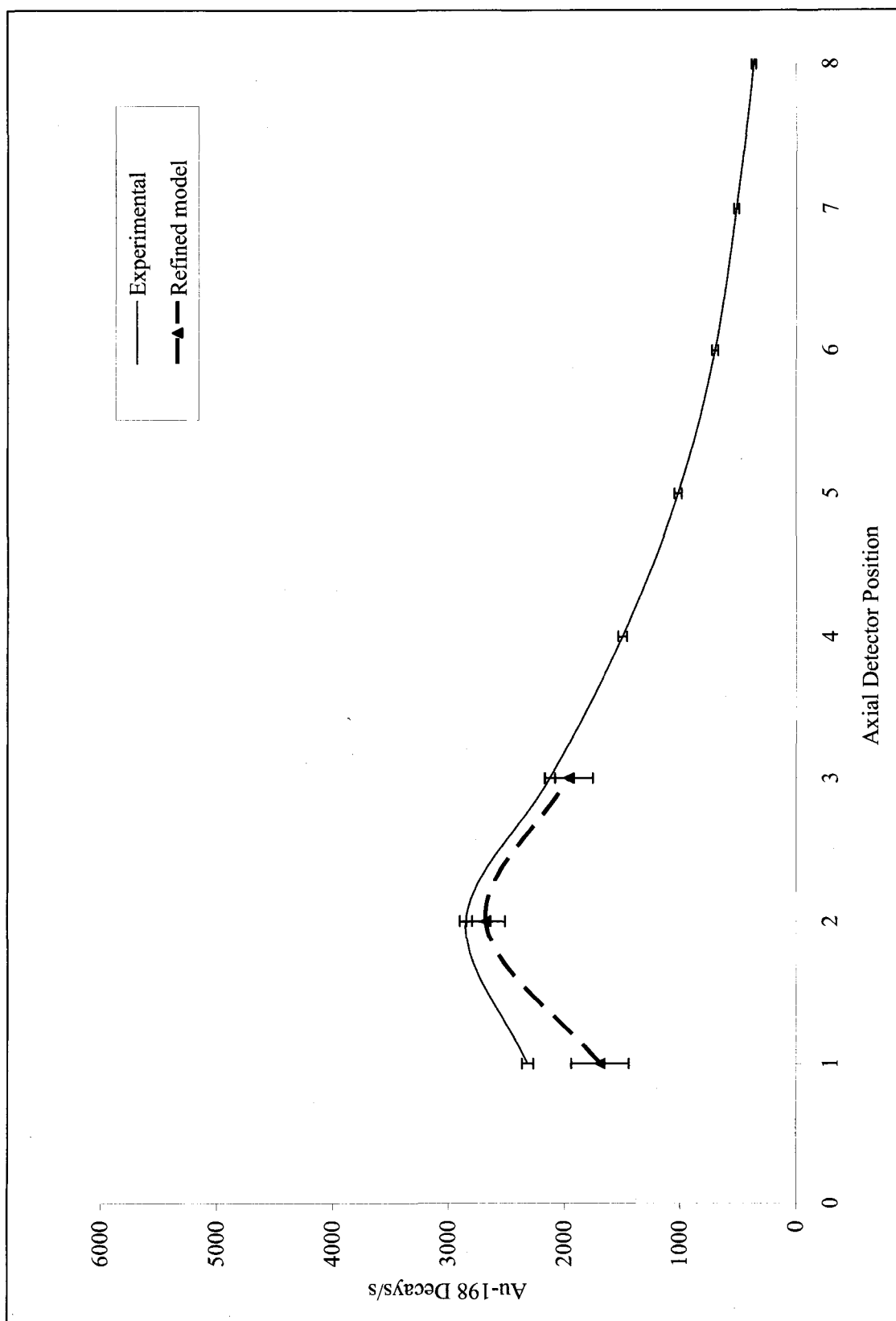


Figure 11 Decay rate comparisons for refined model.

CHAPTER 5

SUMMARY, CONCLUSIONS, AND RECOMMENDATIONS

Discussion of Results

Although the majority of the models produced ^{198}Au decay rates that were significantly larger than those from the experiment, they suggested trends that allowed the creation of a more refined model that provided much better agreement with experiments. The trend toward overestimated fluxes has been seen before in RACE experiments [14] and could be due to several factors, including the alignment of the target with the beam window or a lack of information about materials being used in the experiment. When this experiment was conducted, it was known that the target might not be in perfect alignment with the beam tube. Target alignment could be a significant issue, but in this case, it is not likely that it caused the majority of the deviation from the MCNPX results.

Beam alignment issues have been seen before, even with targets that bolt directly to the beam port like the ISU-RACE and Texas RACE targets. This suggests that there is a more likely cause for the deviation than target alignment problems. Additionally, the deviations have been seen on three different accelerators. The Texas RACE target was found to have beam alignment issues not related to the target/beam port interface. If the electron beam does not exit the beam window in the intended and assumed direction of the target, but rather has some slight angle as it moves through the vacuum tube, then the

target will not receive a beam spot at the location used in the models. Simply being off-center can cause significant changes in reactions within the target, depending on the geometry.

Another significant issue appears to be the modeling of the steel table, polyethylene bricks and the aluminum sheet under the target. The various materials used and the isotopes that make up these materials, particularly in the borated polyethylene, can greatly change the particle interactions within the target. A reflector below the target can send particles back into the target that otherwise might have never come back.

Additionally, materials that are good moderators can slow the neutrons down to the point that they have an increased probability of being absorbed in the gold foils, thus increasing decay rate values. In order to accurately model an experiment, the materials involved must be known and any experiment that is run without this knowledge is an ill-posed problem.

Many of the photo-neutrons created in this target actually come from the tungsten disk stack, itself. The first foil in the series is placed closer to the face of the target than the first tungsten disk, so its activation values were slightly lower than the second foil in both experiments and models where acceptable statistics were achieved.

Conclusions and Recommendations for Further Study

The tungsten disk stack should be altered in order to evenly distribute the beam energy. From the data presented in Table 4 pertaining to the fraction of total energy deposited in the first 4 disks, the total thickness of all disks should be no more than 0.60 cm of tungsten. Nearly all of the electron energy will still be deposited in the tungsten at

this thickness, with the added benefit of moving more of the photons into the uranium fuel rod that this target was designed to use. Photo-neutrons created in the uranium, rather than up front in the tungsten, obviously have an increased opportunity to fission, thus increasing neutron emission. Though the number of neutrons created in the tungsten is comparatively small, even one neutron moved into the uranium rod is of benefit.

The HP-RACE target is not attached to the vacuum port like the ISU RACE target was. In order to maintain the required vacuum within the beam port, the target will have to be placed in front of an electron linear accelerator, but not attached to it. This will require a beam window. At higher energies, the integrity of the beam window will come into question. Just like the target, the temperature of the beam window will increase as the number of particles/s passing through it increases. If the beam window fails, the waveguide or accelerator structure could be damaged [16]. At powers as high as the HP-RACE was designed for, beam window cooling may be required.

Many of these problems can be solved with one simple piece of equipment: a thin, sturdy, telescopic target stand. It should be made of a known material, such as stainless steel, and should be built so that it will hold the target in alignment with the beam tube. This will obviously require advance planning and measuring. This will solve issues associated with beam alignment and unknown composition of materials around the target. The only way to accurately model an experiment is to know everything about the experiment prior to modeling. A simple stand could have removed several unknown variables from this study. With a transportable, adjustable stand and a uranium fuel rod, the HP-RACE target should perform as intended.

APPENDIX

SAMPLE MCNPX INPUT AND OUTPUT FILES

c CELL DESCRIPTION

```

99 0      1 imp:n=0 imp:e=0 imp:p=0 $ Out of This World
1 0      -1 #30 #10 #11 #12 #13 #14 #15 #16 #20
          #40 #41 #42 #43 #44 #45 #46 #47 #48 #25 24
          26 imp:n=1 imp:e=1 imp:p=1 $ Air
2 2 -1.29e-4 -26 imp:n=1 imp:e=1 imp:p=1
10 8 -18.5 -10 33 34 35 36          imp:n=1 imp:e=1 imp:p=1 $ Target D7
11 8 -18.5 -11 33 34 35 36          imp:n=1 imp:e=1 imp:p=1 $ Target D6
12 8 -18.5 -12 33 34 35 36          imp:n=1 imp:e=1 imp:p=1 $ Target D5
13 8 -18.5 -13 33 34 35 36          imp:n=1 imp:e=1 imp:p=1 $ Target D4
14 8 -18.5 -14 33 34 35 36          imp:n=1 imp:e=1 imp:p=1 $ Target D3
15 8 -18.5 -15 33 34 35 36          imp:n=1 imp:e=1 imp:p=1 $ Target D2
16 8 -18.5 -16 33 34 35 36          imp:n=1 imp:e=1 imp:p=1 $ Target D1
20 4 -11.35 -20          imp:n=1 imp:e=1 imp:p=1 $ LEAD
30 9 -2.7 (-27:-28:-29:-30) 33 34 35 36 37 26 imp:n=1 imp:e=1 imp:p=1 $ Al-not the
main body
25 9 -2.7 -25 20 vol=1763.12          imp:n=1 imp:e=1 imp:p=1 $ Al Body -rear
24 9 -2.7 -24 #40 #30 27 28 29 30 20 37 33 34 35 26
          imp:n=1 imp:e=1 imp:p=1          $ Al Body front
40 1 -1 (-37:-33:-34:-35:-36) #10 #11 #12 #13 #14
          #15 #16 #41 #42 #43 #44 #45 #46 #47 #48
          imp:n=1 imp:e=1 imp:p=1          $ Water
41 9 -2.7 -45 (-43:-41:-39:-38:-42:-44) 40 46 47 48 49
          imp:n=1 imp:e=1 imp:p=1          $ Al Spacer
42 like 41 but *trcl=(0 0 .66 -90 180 90 0 -90 90 -90 90 0)
43 like 41 but *trcl=(0 0 1.2)
44 like 41 but *trcl=(0 0 1.67 -90 180 90 0 -90 90 -90 90 0)
45 like 41 but *trcl=(0 0 2.1)
46 like 41 but *trcl=(0 0 2.5 -90 180 90 0 -90 90 -90 90 0)
47 like 41 but *trcl=(0 0 2.88)
48 like 41 but *trcl=(0 0 3.25 -90 180 90 0 -90 90 -90 90 0)

```

c SURFACE DEFINITIONS

```

1 SPH 0 0 0      50          $ Air Sphere
10 RCC 0 0 5.75 0 0 0.41 3    $ Tungsten D7
11 RCC 0 0 6.41 0 0 0.29 3    $ Tungsten D6

```


12 RCC 0 0 6.95 0 0 0.22 3	\$ Tungsten D5
13 RCC 0 0 7.42 0 0 0.18 3	\$ Tungsten D4
14 RCC 0 0 7.85 0 0 0.15 3	\$ Tungsten D3
15 RCC 0 0 8.25 0 0 0.13 3	\$ Tungsten D2
16 RCC 0 0 8.63 0 0 0.12 3	\$ Tungsten D1
20 RCC 0 0 -16.3 0 0 21.3 1.232	\$ U Plug .036 cm Al Sleeve
25 RCC 0 0 -17.8 0 0 23 5.08	\$ Al Block rear
24 RCC 0 0 5.2 0 0 5.3 5.08	\$ Al Block
26 RCC 0 0 9.3 0 0 1.2 1.74	\$ Hole in Face
27 RCC 0 3 10.4 0 0 2.55 1.25	\$ Al Water Connection
28 RCC 0 -3 10.4 0 0 2.55 1.25	\$ Al Water Connection
29 RCC 3 0 10.4 0 0 2.55 1.25	\$ Al Water Connection
30 RCC -3 0 10.4 0 0 2.55 1.25	\$ Al Water Connection
33 RCC 0 3 5.5 0 0 7.45 0.635	\$ Water Channel
34 RCC 0 -3 5.5 0 0 7.45 0.635	\$ Water Channel
35 RCC 3 0 5.5 0 0 7.45 0.635	\$ Water Channel
36 RCC -3 0 5.5 0 0 7.45 0.635	\$ Water Channel
37 RCC 0 0 5.5 0 0 3.5 3.01	\$ Water
38 RCC 1.5 0 5.5 0 0 0.25 1.5	\$ Al Spacer
39 RCC -1.5 0 5.5 0 0 0.25 1.5	\$ Al Spacer
40 RCC 0 0 5.5 0 0 0.25 1.8	\$ Al Spacer
41 RCC -4.128 3.24 5.5 0 0 0.25 3.55	\$ Al Spacer
42 RCC 4.128 3.24 5.5 0 0 0.25 3.55	\$ Al Spacer
43 RCC -4.128 -3.24 5.5 0 0 0.25 3.55	\$ Al Spacer
44 RCC 4.128 -3.24 5.5 0 0 0.25 3.55	\$ Al Spacer
45 RCC 0 0 5.5 0 0 0.25 3	\$ Al Spacer
46 Rcc -3 0 5.5 0 0 0.25 0.635	\$ Al Spacer
47 Rcc 3 0 5.5 0 0 0.25 0.635	\$ Al Spacer
48 Rcc 0 3 5.5 0 0 0.25 0.635	\$ Al Spacer
49 Rcc 0 -3 5.5 0 0 0.25 0.635	\$ Al Spacer
m1 8016 1 1001.60c 2	\$ water
MT1 lwtr.01t	
m2 7014 79 8016 21 gas=1	\$ Air
m4 82208 1	\$ lead 11.35
m8 74182 -0.198735 74183 -0.1074 74184 -0.23 74186 -0.2132	
29063 -0.1730 29065 -0.077665	\$ W-Cu Target -18.5
m9 13027 98 24052 0.04 29065 0.15 26056 0.7 12024 0.8 25055 0.15 14028 0.4	
81204 0.15	\$ Al-27 2.7
nps 1e8	
mode n e p	

```

SDEF ERG=d1 POS 0 0 10.49 PAR=e AXS 0 0 -1 vec 0 0 1 dir -1
sil L 17 17.5 18 18.5 19 19.5 20 20.5 21 21.5 22 22.5 23
    23.5 24 24.5 25 25.5 26 26.5 27 27.5 28 28.5
sp1 0.00302 0.00359 0.00395 0.00543 0.00571 0.00747 0.00879
    0.01087 0.01392 0.02445 0.05931 0.10735 0.14278 0.14292
    0.12676 0.10129 0.07426 0.05456 0.03879 0.02788 0.01973
    0.01166 0.00482 0.00069
Phys:p 3j 1
cut:p j 5
cut:e j 5
prdmp 2j 1
f2:n 25.1
e2 1e-8 2e-8 3e-8 4e-8 5e-8 6e-8 7e-8 8e-8 9e-8 1e-7 2e-7
    3e-7 4e-7 5e-7 6e-7 7e-7 8e-7 9e-7 1.00E-06 1.00E-05
    1.00E-04 1.00E-03 1.00E-02
    2.00E-02 3.00E-02 4.00E-02 5.00E-02 6.00E-02 7.00E-02
    8.00E-02 9.00E-02 1.00E-01
    2.00E-01 3.00E-01 4.00E-01 5.00E-01 6.00E-01 7.00E-01
    8.00E-01 9.00E-01 1.00 1 1.1 1.2 1.3 1.4 1.5 1.6 1.7
    1.8 1.9 2 2.1 2.2 2.3 2.4 2.5 2.6 2.7 2.8 2.9 3 3.1
    3.2 3.3 3.4 3.5 3.6 3.7 3.8 3.9 4 4.1 4.2 4.3 4.4 4.5
    4.6 4.7 4.8 4.9 5 5.1 5.2 5.3 5.4 5.5 5.6 5.7 5.8 5.9
    6 6.1 6.2 6.3 6.4 6.5 6.6 6.7 6.8 6.9 7 7.1 7.2 7.3
    7.4 7.5 7.6 7.7 7.8 7.9 8 8.1 8.2 8.3 8.4 8.5 8.6 8.7
    8.8 8.9 9 9.1 9.2 9.3 9.4 9.5 9.6 9.7 9.8 9.9 10
sd2 1
c mesh geom=cyl ref=0 0 10.49 origin=.001 .001 13 axs=0 0 -1 vec=1 0 0
c imesh 10 iints 20 jmesh 31.1 jints 20 kmesh 1 kints 13
c wwg 2 0
wwp:n 4j -1
wwp:p 4j -1
print

```

Energy output file (cut for brevity)

total 65253465 1.00000E+00 5.03866E-04 1.00000E+00
 tally 2 nps =100000000
 tally type 2 particle flux averaged over a surface. units 1/cm**2
 particle(s): neutron

areas
 surface: 25.1
 1.00000E+00

surface 25.1

energy
 1.0000E-08 3.37208E-08 0.0504
 2.0000E-08 8.02244E-08 0.0337
 3.0000E-08 1.02565E-07 0.0256
 4.0000E-08 1.20931E-07 0.0273
 5.0000E-08 1.20867E-07 0.0239
 6.0000E-08 1.24411E-07 0.0229
 7.0000E-08 1.21280E-07 0.0256
 8.0000E-08 1.15692E-07 0.0236
 9.0000E-08 1.03527E-07 0.0277
 1.0000E-07 9.30760E-08 0.0323
 2.0000E-07 7.27060E-07 0.0108
 3.0000E-07 4.98562E-07 0.0122
 4.0000E-07 4.05342E-07 0.0148
 5.0000E-07 3.41850E-07 0.0137
 6.0000E-07 3.13743E-07 0.0165
 7.0000E-07 2.77404E-07 0.0179
 8.0000E-07 2.47393E-07 0.0190
 9.0000E-07 2.27987E-07 0.0172
 1.0000E-06 2.19845E-07 0.0175
 1.0000E-05 6.83442E-06 0.0035
 1.0000E-04 1.61118E-05 0.0022
 1.0000E-03 3.83820E-05 0.0015
 1.0000E-02 8.90443E-05 0.0010
 2.0000E-02 4.32212E-05 0.0013
 3.0000E-02 4.55269E-05 0.0013
 4.0000E-02 1.84858E-05 0.0021
 5.0000E-02 1.97350E-05 0.0020
 6.0000E-02 2.26152E-05 0.0018
 7.0000E-02 3.10337E-05 0.0016
 8.0000E-02 3.56819E-05 0.0015
 9.0000E-02 7.88276E-06 0.0031
 1.0000E-01 9.51067E-06 0.0028
 2.0000E-01 1.80467E-04 0.0008

3.0000E-01	1.61708E-04	0.0008
4.0000E-01	1.64189E-04	0.0008
5.0000E-01	1.35773E-04	0.0008
6.0000E-01	1.35011E-04	0.0008
7.0000E-01	1.34352E-04	0.0008
8.0000E-01	1.23210E-04	0.0009
9.0000E-01	9.32444E-05	0.0010
1.0000E+00	9.41301E-05	0.0010
1.0000E+00	0.00000E+00	0.0000
1.1000E+00	8.80405E-05	0.0010
1.2000E+00	6.85251E-05	0.0011
1.3000E+00	6.33732E-05	0.0012
1.4000E+00	5.93112E-05	0.0012
1.5000E+00	4.96237E-05	0.0013
1.6000E+00	4.26142E-05	0.0014
1.7000E+00	3.94808E-05	0.0015
1.8000E+00	3.21225E-05	0.0016
1.9000E+00	3.26183E-05	0.0016
2.0000E+00	2.63336E-05	0.0018
2.1000E+00	2.23600E-05	0.0019
2.2000E+00	2.05316E-05	0.0020
2.3000E+00	1.81183E-05	0.0021
2.4000E+00	1.74155E-05	0.0022
2.5000E+00	1.63985E-05	0.0023
2.6000E+00	1.20179E-05	0.0026
2.7000E+00	1.15769E-05	0.0026
2.8000E+00	1.00257E-05	0.0028
2.9000E+00	9.52445E-06	0.0030
3.0000E+00	8.22901E-06	0.0032
3.1000E+00	7.49360E-06	0.0033
3.2000E+00	6.88771E-06	0.0034
3.3000E+00	5.96877E-06	0.0036
3.4000E+00	5.43429E-06	0.0039
3.5000E+00	5.04051E-06	0.0040
3.6000E+00	4.56127E-06	0.0047
3.7000E+00	4.17181E-06	0.0074
3.8000E+00	3.74082E-06	0.0045
3.9000E+00	3.62811E-06	0.0047
4.0000E+00	3.37521E-06	0.0049
4.1000E+00	3.08997E-06	0.0049
4.2000E+00	2.89182E-06	0.0051
4.3000E+00	2.79974E-06	0.0052
4.4000E+00	2.45869E-06	0.0055
4.5000E+00	2.47615E-06	0.0057
4.6000E+00	2.29034E-06	0.0057
4.7000E+00	2.12759E-06	0.0059

4.8000E+00	2.01711E-06	0.0060
4.9000E+00	1.94471E-06	0.0061
5.0000E+00	1.84290E-06	0.0063
5.1000E+00	1.66742E-06	0.0064
5.2000E+00	1.57794E-06	0.0068
5.3000E+00	1.59225E-06	0.0067
5.4000E+00	1.43761E-06	0.0071
5.5000E+00	1.38371E-06	0.0070
5.6000E+00	1.31461E-06	0.0072
5.7000E+00	1.22457E-06	0.0075
5.8000E+00	1.19224E-06	0.0075
5.9000E+00	1.10274E-06	0.0078
6.0000E+00	1.01361E-06	0.0080
6.1000E+00	9.63558E-07	0.0084
6.2000E+00	9.26484E-07	0.0083
6.3000E+00	8.89884E-07	0.0088
6.4000E+00	8.30774E-07	0.0088
6.5000E+00	7.71856E-07	0.0093
6.6000E+00	7.53157E-07	0.0096
6.7000E+00	6.97798E-07	0.0100
6.8000E+00	6.35948E-07	0.0098
6.9000E+00	6.11011E-07	0.0099
7.0000E+00	5.77860E-07	0.0106
7.1000E+00	5.50453E-07	0.0109
7.2000E+00	5.11845E-07	0.0111
7.3000E+00	4.88144E-07	0.0119
7.4000E+00	4.47183E-07	0.0118
7.5000E+00	4.34494E-07	0.0120
7.6000E+00	4.08636E-07	0.0121
7.7000E+00	3.75324E-07	0.0126
7.8000E+00	3.62958E-07	0.0131
7.9000E+00	3.33346E-07	0.0134
8.0000E+00	3.10848E-07	0.0136
8.1000E+00	2.96625E-07	0.0141
8.2000E+00	2.70738E-07	0.0152
8.3000E+00	2.61834E-07	0.0149
8.4000E+00	2.38617E-07	0.0158
8.5000E+00	2.25898E-07	0.0159
8.6000E+00	2.14477E-07	0.0163
8.7000E+00	1.98460E-07	0.0174
8.8000E+00	1.82690E-07	0.0176
8.9000E+00	1.72708E-07	0.0179
9.0000E+00	1.58350E-07	0.0191
9.1000E+00	1.49986E-07	0.0193
9.2000E+00	1.41973E-07	0.0197
9.3000E+00	1.30794E-07	0.0215

9.4000E+00	1.23255E-07	0.0211
9.5000E+00	1.15319E-07	0.0232
9.6000E+00	1.05333E-07	0.0232
9.7000E+00	9.70987E-08	0.0246
9.8000E+00	9.02824E-08	0.0245
9.9000E+00	8.45626E-08	0.0254
1.0000E+01	7.64381E-08	0.0269
total	2.36163E-03	0.0004

BIBLIOGRAPHY

1. LeCounte, R.D., Beller, T.E., Howard B., Beller, D.E., and Cook, D., "Design of the High-Power RACE Target," *Proceedings of the Eighth International Topical Meeting on Nuclear Applications and Utilization of Accelerators*, 30 July-2 August 2007, Pocatello, Idaho.
2. MCNPX Team, *MCNPX User's Manual, Version 2.6D*, Los Alamos National Laboratory report, LA-UR-07-4137, June 2007.
3. Galassi, G., 2003, "UNLV Transmutation Research Program Strives to Improve Safety of Nuclear Waste," *Inside UNLV*, December issue.
4. Browne, E. et al., 1978, *Table of Radioactive Isotopes, Seventh Edition*, Wiley-Interscience, Hoboken, New Jersey, pp. 1271
5. Baum, E.M., Knox, H.D., and Miller, T.R., 2002, *Nuclides and Isotope, Chart of the Nuclides, 16th Edition*, KAPL, Inc., pp. 53, 65, 88.
6. Salvatores M., et al., "TRADE (TRIGA Accelerator Driven Experiment): A Full Experimental Validation of the ADS Concept in a European Perspective," *Proceedings of the Sixth International Meeting on Nuclear Applications of Accelerator Technology*, AccApp'03, American Nuclear Society, 2004, p. 8-16.
7. Gohar, Y., "Design and Analyses of Electron Tungsten Targets for Neutron Generation", presented at the *Fourth Annual ADSS Experiments Workshop*, Texas A&M University on 11-14 April 2006.
8. Beller, D.E., "Overview of the AFCI Reactor-Accelerator Coupling Experiments (RACE) Project," *Proceedings of the Eighth Information Exchange Meeting on Actinide and Fission Product Partitioning & Transmutation* (OECD/NEA), 9-11 November 2004, Las Vegas, Nevada.
9. Beller, D.E., "AFCI Reactor-Accelerator Coupling Experiments (RACE) Project Overview," presented at the *3rd Annual ADSS Experiments Workshop*, Pocatello, Idaho, 1 June 2005.
10. O'Kelly, S., "Accelerator Driven Accelerator Driven Subcritical Experiments at Subcritical Experiments at the University of Texas ", *Proceedings of the Joint Meeting of the National Organization of Test, Research, and Training Reactors and*

the International Group on Research Reactors, 12-16 September 2005, Gaithersburg, MD.

11. T. Beller, B. Howard, R. LeCounte, and D. Beller, "High-Power Accelerator Target Design for the AFCI RACE Project," *Proceedings of the 2006 International High Level Radioactive Waste Management Conference*, Las Vegas, NV, pp. 1244-1246 (2006). (Available on CD-ROM from the American Nuclear Society).
12. Lamarsh, J.R. and Barratta, A.J., 2001, *Introduction to Nuclear Engineering*, Prentice Hall, New Jersey, pp. 82, 88, 738, 741-742.
13. Krane, K.S., *Introductory Nuclear Physics*, John Wiley and Sons, Inc., Hoboken, New Jersey, pp. 65 and inside back cover.
14. O'Kelly, S., "RACE RACE-LP at The University of LP at The University of Texas: Texas: Lessons Learned", presented at the Fourth Annual ADSS Experiments Workshop, Texas A&M University on 11-14 April 2006.
15. Thermo Electron Corporation, "Shielding Solutions for the 21st Century", Catalog 26, Santa Fe, NM, pp. 10-12.
16. *Vacuum System*, Stanford Linear Accelerator Center, accessed 27 October 2007, <http://www2.slac.stanford.edu/vvc/accelerators/vacuum.html>.

VITA

Graduate College
University of Nevada, Las Vegas

Timothy Eugene Beller

Home Address:

459 Linn Ln
Las Vegas, Nevada 89110

Degrees:

Bachelor of Science in Mechanical Engineering, 2006
University of Nevada, Las Vegas

Publications:

T. Beller, D. Curtis, D. Beller, A. Rimsky-Korsakov, and T. Ward, "The UNLV Neutron Multiplicity Detector System," *Proceedings of the Eighth Information Exchange Meeting on Actinide and Fission Product Partitioning & Transmutation*, OECD/NEA, Paris, France, pp 687-698 (2005).

T. Beller, B. Howard, R. LeCounte, and D. Beller, "High-Power Accelerator Target Design for the AFCI RACE Project," *Proceedings of the 2006 International High Level Radioactive Waste Management Conference*, Las Vegas, NV, pp. 1244-1246 (2006). (Available on CD-ROM from the American Nuclear Society).

Thesis Title: Neutronics Analysis of the High-Power Race Target

Thesis Examination Committee:

Chairperson, Dr. Daniel Cook, Ph. D.
Committee Member, Dr. Charlotta Sanders, Ph. D., P.E.
Committee Member, Dr. Woosoon Yim, Ph. D.
Graduate Faculty Representative, Dr. Julie Staggers, Ph. D.